

Heat transfer mechanism driven by acoustic body force under acoustic fields

Varun Kumar,¹ Mohammed Azharudeen,¹ Charish Pothuri,² and Karthick Subramani^{1,*}

¹*Department of Mechanical Engineering, Indian Institute of Information Technology, Design and Manufacturing Kancheepuram, Chennai-600127, India*

²*Department of Mechanical Engineering, Shiv Nadar University, Gautam Buddha Nagar, Uttar Pradesh-201314, India*



(Received 14 January 2021; accepted 25 June 2021; published 15 July 2021)

In this paper, we demonstrate a heat transfer mechanism using ultrasonic standing waves. The basic idea behind the proposed heat transfer mechanism is the acoustic relocation phenomenon of inhomogeneous fluid due to acoustic body force. The acoustic body force depends upon the density gradient and the speed of the sound gradient of the inhomogeneous fluid. Heating a fluid creates an inhomogeneity in the physical properties of the fluid such as density, viscosity, and velocity of sound, etc. When this heated (inhomogeneous) fluid is subjected to ultrasonic standing waves, acoustic body force induces a fluid motion which is shown to be responsible for this heat transfer mechanism. Heat transfer enhancement is observed when a standing acoustic wave is passed perpendicular to the direction of heat transfer. Remarkably, it is found that acoustic forces can enhance heat transfer up to 2.5 times compared to natural convection and up to 11.2 times compared to pure conduction. Suppression of natural convection heat transfer is observed when the acoustic waves are passed parallel to the direction of heat transfer. In this case, acoustic forces could bring down the heat transfer by half or more than half from the natural convection. To characterize the heat transfer mechanism in the enhancement case, a modified Rayleigh number that can account for both acoustics and gravity effects is proposed. To this extent, we provide a clear understanding of how acoustic fields influence the fluid flow and heat transfer.

DOI: [10.1103/PhysRevFluids.6.073501](https://doi.org/10.1103/PhysRevFluids.6.073501)

I. INTRODUCTION

Since the advent of miniaturization, the removal of heat from a microsystem to keep the temperature in operating conditions has been an important challenge in the field of heat transfer. Researchers have employed various thermal management techniques to address this problem, including heat sinks, heat pipes, thermoelectric (Peltier) coolers, synthetic jet cooling, thermosyphons, phase change materials, electro-osmotic pumping, microchannels, nanofluids, ferrofluids, and impinging jets [1]. Although significant progress has been made, there is an increasing demand for innovative cooling strategies due to emerging high heat flux electronic devices. Other important applications such as cooling of microsystems in a microgravity environment (space) pose a unique challenge of heat transport without natural convection or gravity [2].

There have been active studies on the effects of acoustic fields on convective heat transfer since the 1960s [3]. To enhance the heat transport, researchers have employed many acoustic phenomena such as acoustic streaming [4–6], acoustic cavitation [7], acoustic local agitation [8], and the acoustic release of vapor bubbles (boiling heat transfer) [3]. Among them, the widely investigated

*karthick@iiitdm.ac.in

acoustic phenomena to enhance heat transfer are acoustic streaming and acoustic cavitation. Acoustic streaming is a steady circular flow in the fluid domain subjected to high-intensity acoustic fields. Acoustic cavitation refers to the formation, growth, and violent collapse of gas bubbles into the liquid under the acoustic fields.

In light of recent experiments, it was discovered that the acoustic forces acting on inhomogeneous fluids (nonuniform density and velocity of sound) exhibit an intriguing phenomenon called acoustic relocation [9]. Using bulk acoustic standing waves, Deshmukh *et al.* demonstrated the acoustic relocation phenomenon by relocating higher impedance (product of density and speed of the sound) fluid from the wall to the center of the microchannel and also stabilized the concentration profiles against hydrostatic pressure gradients due to gravitational forces [9]. Following the above experiments, Karlsen *et al.* provided a theoretical explanation of this acoustic relocation phenomenon using the theory of nonlinear acoustics [10]. They also derived a mathematical equation for the second-order acoustic body force called acoustic force density which is responsible for the relocation of inhomogeneous fluids. Furthermore, this acoustic body force is employed in several applications such as cell handling through iso-acoustic focusing [11], acoustic impedance-based circulating tumor cell isolation from blood [12], acoustic mixing of inhomogeneous fluids [13], and separation of bacteria (submicron particles) from blood lysate through gradient acoustic focusing [14]. Here, we aim to exploit this acoustic body force which is responsible for acoustic relocation in the arena of heat transfer.

From the above experiments and theory, it is evident that acoustic forces can create bulk fluid motion or relocation if the flow field has a density gradient or speed of sound gradient. It is also a well-known fact that the physical properties such as density and velocity of sound depend on temperature. Since all the heat transfer processes (convective) involve temperature gradients, it will also have density and speed of sound gradients [15]. Thus, we hypothesize that when the heated fluid domain (with temperature gradient) is subjected to a standing acoustic wave, acoustic body forces can produce bulk fluid motion which can serve as a potential heat transfer mechanism.

The main goal of this paper is to demonstrate a heat transfer mechanism based on the acoustic relocation phenomenon under acoustic fields. The effect of acoustic forces on the heat transfer process is studied with and without the presence of gravity. Previous works on acoustic streaming due to temperature variation only focused on the gases and the effect of density variation on heat transfer alone is considered, the effect of speed of sound variation on the acoustic streaming is neglected [6] whereas our theory applies to both gases and liquids. Also, the effect of both the density variation and speed of sound variation on heat transfer is considered. The present paper sheds light on the interplay among the temperature field, velocity field, and acoustic body force.

II. PHYSICS OF THE PROBLEM

In this section, we outline the main idea or physics behind the proposed heat transfer mechanism using acoustic standing waves. Before understanding the physics involved, it is important to gain prior knowledge of the acoustic relocation phenomenon observed in the inhomogeneous fluids. Recently, it was discovered that when an inhomogeneous fluid is subjected to an acoustic standing wave, the inhomogeneous fluid is relocated/moved to a stable-field configuration. It was shown that the acoustic body force which is responsible for this acoustic relocation phenomenon is a function of density gradient and speed of sound gradient [10].

The acoustic relocation behavior of inhomogeneous fluids from the initial configuration to a stable configuration is clearly illustrated in Fig. 1. An acoustic standing half wave of wavelength $\lambda = 2w$ is applied along the X axis or width direction, where w is the width of the channel in the X direction and h is the height of the channel in the Y direction. Due to the hard wall boundary conditions, pressure nodes are formed at the center and pressure antinodes are formed at the sidewalls as shown in Fig. 1. For the sake of understanding and to simplify the arguments, in this section we shall assume that inhomogeneous fluid considered has only density gradient and negligible speed of sound gradient. In the later sections, the effect of the speed of sound gradient

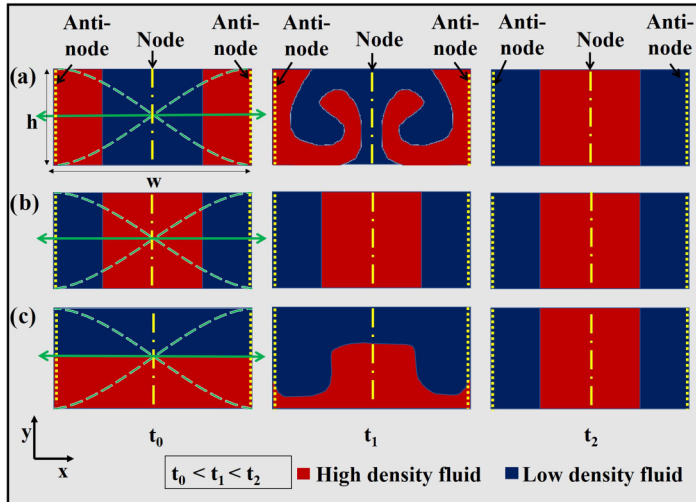


FIG. 1. Acoustic relocation phenomenon in the inhomogeneous fluids of different configurations subjected to acoustic standing half waves. (a) High-density fluid initially at sides (antinode). (b) High-density fluid initially at the center (node) and (c) high-density fluid initially at the bottom. Green dotted lines indicate standing half waves whereas the green arrow indicates the direction of standing half waves. The yellow long dot-dashed line indicates node (center) and the yellow short dashed line indicates antinode (sidewalls).

shall be accounted for. Since the fluid has inhomogeneous density, the acoustic body force moves high-density fluid to the pressure nodes (center) and low-density fluid to the pressure antinode (walls). Hence the configuration of a high-density fluid at the node/center and low density at the antinode/wall is called a stable configuration, as shown in Fig. 1(a). The fluid configurations other than stable configurations are called unstable configurations. A few examples of unstable configurations are high density at the sides/low density at the center and high density at the bottom/low density at the top as shown in Figs. 1(a) and 1(c) at time $t = t_0$. When the unstable configurations are subjected to acoustic standing half wave, acoustic force relocates inhomogeneous fluid to the stable configuration as illustrated in Figs. 1(a) and 1(c) at time $t = t_2$. Once the fluid is relocated to a stable configuration, the fluid motion ceases to exist. If the initial configuration of the fluid is already stable, then this stable configuration remains unchanged under the acoustic standing half wave as shown in Fig. 1(b).

The proposed heat transfer mechanism is based on two facts: First, the thermophysical properties are a function of temperature. Thus, heating the fluid (temperature gradient) creates inhomogeneity in the physical properties of the fluid such as density gradient [16], the velocity of the sound gradient [17], viscosity gradient [18], and thermal conductivity [19]. Second, acoustic forces can relocate the fluid configuration if there exists a density gradient or velocity of the sound gradient in the flow field as discussed in Fig. 1. The schematic representation of the heat transfer mechanism using ultrasonic waves is shown in Fig. 2. The bottom wall is maintained at a higher temperature (T_H) compared to the top wall (T_L) of the channel and the side walls are insulated. The presence of the high-temperature wall at the bottom generates the fluid with the lowest density (dark blue circle) and fluid with the highest density (dark red) is at the top of the channel due to the presence of the low temperature at the top wall. When the channel is subjected to ultrasonic acoustic waves parallel to the width direction, the acoustic body force acting on the fluid relocates the low-density fluid at the bottom toward the side wall (antinodes) and high-density fluid at the top toward the center of the channel. This causes fluid circulation as follows: bottom → side → top → center → bottom as shown in Fig. 2. Since the fluid is continuously heated in the presence of the acoustic field, the process of fluid circulation always exists, unlike the relocation shown in Fig. 1. This fluid circulation

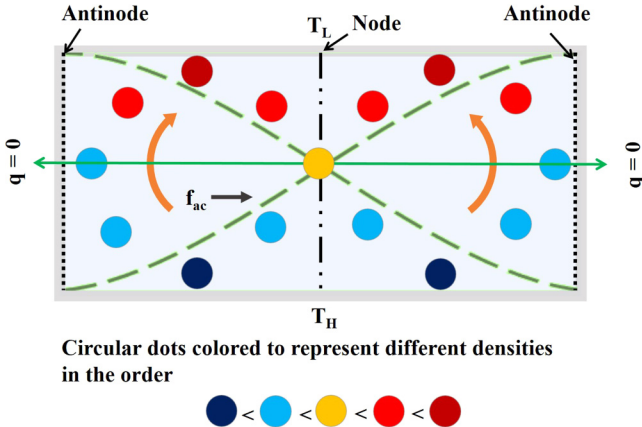


FIG. 2. Schematic representation of the proposed heat transfer mechanism based on acoustic relocation phenomenon.

due to acoustic body force gives rise to convective heat transfer mechanism, which is different from natural convection where the fluid motion is due to gravity. The above discussion clearly outlines the main idea behind the proposed heat transfer mechanism.

III. THEORETICAL MODEL

A. Model setup

Though the acoustic relocation phenomenon (Fig. 1) was studied only in a microchannel ($\approx 400 \mu\text{m}$) [10], the proposed heat transfer mechanism based on the acoustic relocation phenomenon is demonstrated in a minichannel. The reason for using a minichannel over a microchannel is convection effects due to body force such as gravity become unimportant in a microchannel. Thus, a simple two-dimensional (2D) minichannel enclosure of width (w) 8 mm and height (h) 4 mm is considered as shown in Figs. 3(a) and 3(b). Initially, the fluid domain is kept at rest. This fluid domain or enclosure is maintained at a higher temperature at the bottom ($T(x, -\frac{h}{2}) = 320 \text{ K}$) and at a lower temperature at the top ($T(x, +\frac{h}{2}) = 290 \text{ K}$). Thus, an inhomogeneity is caused in density ($\rho(x, y)$) and the speed of sound ($c(x, y)$). Water and ethanol have been considered as the working fluids in this study. The minichannel taken for this analysis is subjected to acoustics in two different directions with respect to the direction of the heat transfer.

(1) An acoustic standing half wave of wavelength $\lambda = 2w$ is applied along the X axis or width direction as shown in Fig. 3(a). Here the pressure nodes are formed at the center (parallel to the Y axis) and pressure antinodes are formed at sidewalls.

(2) An acoustic standing half wave of wavelength $\lambda = 2h$ is applied along the Y axis or height direction as shown in Fig. 3(b). Here the pressure nodes are formed at the center (parallel to the X axis) and pressure antinodes are formed at the top and bottom walls.

Both these configurations are tested at without gravity ($g = 0$) and with gravity ($g = 9.81 \text{ m/s}^2$) conditions, where the acceleration due to gravity is considered only in the Y axis is taken as $g_y = -g \vec{j}$.

B. Governing equations

The unsteady laminar natural convection problem is governed by continuity, momentum equation, and energy equation [20]. In this problem, temperature change induces fluid flow through the buoyancy (gravity) and acoustic forces. Then the flow field in turn affects the temperature field

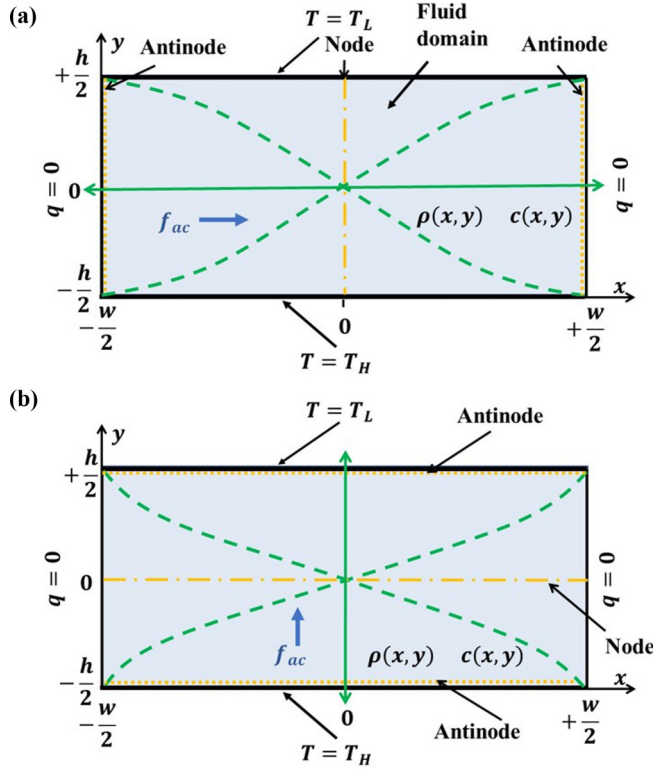


FIG. 3. Schematic of the 2D minichannel of width 8 mm along \$x\$ direction and height of 4 mm in the \$y\$ direction. (a) Acoustic standing half wave applied along X axis or perpendicular to the direction of heat transfer. (b) Acoustic standing half-wave applied along Y axis or parallel to the direction of heat transfer.

through heat transfer. So, the continuity equation, Navier Stokes equations, and energy equation are coupled and have to be solved simultaneously. The continuity equation and Navier Stokes equations are employed in the model as follows:

$$\frac{\partial \rho}{\partial t} + \nabla \cdot (\rho u) = 0, \quad (1)$$

$$\rho \left(\frac{\partial u}{\partial t} \right) + \rho (u \cdot \nabla) u = \nabla \cdot \left(-p + \mu(\nabla u + (\nabla u)^T) - \frac{2}{3}\mu(\nabla \cdot u)I \right) + f_b + f_{ac}, \quad (2)$$

where \$u\$ is the fluid velocity, \$p\$ is the fluid pressure, \$\rho\$ is the fluid density, \$\mu\$ is the fluid viscosity, \$I\$ is the identity matrix, \$f_b = \rho g_y\$ is the body force due to gravity, \$g_y\$ is the acceleration due to gravity, and \$f_{ac}\$ is the acoustic body force acting on the fluid due to the acoustic field. The above equations have to be solved with the following energy equation:

$$\rho C_p \frac{\partial T}{\partial t} + \rho C_p u \cdot \nabla T = \nabla \cdot (k \nabla T), \quad (3)$$

where \$T\$ is temperature field, \$C_p\$ is the specific heat capacity of the fluid, and \$k\$ is the thermal conductivity of the fluid. The above energy equation is a special case in which there is no internal heat generation, negligible viscous dissipation, and negligible compressibility effect [21]. It is important to note that in this model, all thermophysical and acoustic properties [11,15] are allowed to vary with respect to temperature. At the wall, the velocity of the fluid is taken as zero because of the no-slip condition [12]. This problem is assumed to be laminar because the

modified Rayleigh number used in this study is $\lesssim 10^6$, which is less than the critical Reynolds number for turbulence [22]. For an unsteady heat flux over space and time, we use spatiotemporal average heat flux where the spatial average heat flux is defined as average local heat flux at $y = \pm \frac{h}{2}$ over the width w , $q_w = \frac{1}{w} \int_{-\frac{w}{2}}^{\frac{w}{2}} q_{y=\pm\frac{h}{2}} dx$ and the spatiotemporal average heat flux \bar{q}_w are both the time and the spatial average of local heat flux at $y = \pm \frac{h}{2}$ over the width w and time Δt , $\bar{q}_w = \frac{1}{(t_2-t_1)*w} \int_{t_1}^{t_2} \int_{-w/2}^{w/2} q_{y=0} dx dt$. The nondimensional numbers governing the physics of the problem are the Nusselt number (Nu) and Rayleigh number (Ra). The spatiotemporal average Nusselt number $\overline{\text{Nu}}_w$ is taken as $\frac{\bar{h}_w h}{k}$. The spatiotemporal average heat transfer coefficient \bar{h}_w is taken as $\frac{\bar{q}_w}{\Delta T}$, where ΔT is $T(x, -\frac{h}{2}) - T(x, +\frac{h}{2})$.

C. Modeling of acoustic body force

Earlier, the relocation of miscible [9] and immiscible [23] inhomogeneous fluids to the specific stable configuration by the acoustic fields in the microchannel was demonstrated. This phenomenon was explained using the time-averaged second-order acoustic force density which stems from the theory of nonlinear acoustics. The time-averaged second-order acoustic force density can be defined as the divergence of time-averaged acoustic momentum flux density tensor [24]:

$$f_{ac} = -\nabla \cdot \langle \Pi \rangle. \quad (4)$$

The time-averaged acoustic momentum flux density tensor is defined by the first-order acoustic fields $\langle \Pi \rangle = \langle p_2 \rangle \mathbf{I} + \langle \rho_0 \mathbf{v}_1 \mathbf{v}_1 \rangle$, where p_2 is second-order mean Eulerian pressure defined by first-order acoustic fields and is given as $p_2 = \frac{1}{4}\kappa_0|p_1|^2 - \frac{1}{4}\rho_0|\mathbf{v}_1|^2$. κ_0 is the compressibility and ρ_0 is the density of the fluid domain. Compressibility κ_0 is defined as $\frac{1}{(\rho_0 c_0)^2}$. p_1 and \mathbf{v}_1 are first-order acoustic pressure and velocity fields. Using the above equations, the acoustic energy density acting on the inhomogeneous fluid can be derived in terms of the density and compressibility gradient [25],

$$f_{ac} = -\frac{1}{4}|p_1|^2 \nabla \kappa_0 - \frac{1}{4}|\mathbf{v}_1|^2 \nabla \rho_0. \quad (5)$$

The first-order pressure field and velocity field in a weakly inhomogeneous fluid due to acoustic standing half of pressure amplitude p_a applied in the x direction take the form $p_1 = p_a \sin(k_\lambda x)$ and $\mathbf{v}_1 = (\frac{p_a}{\rho_0 c}) \cos(k_\lambda x)$, where $k_\lambda = \frac{2\pi}{\lambda}$ is the wave number and λ is the wavelength of the wave. Since a half wave is employed in this simulation, λ is taken as $2w$. After substituting p_1 , \mathbf{v}_1 , and κ_0 in Eq. (5), we arrive at the final equation for acoustic force density f_{ac} in terms of density and the speed of sound gradient [10],

$$f_{ac} = -E_{ac}(\cos(2k_\lambda x)\nabla \hat{\rho} + (1+\cos(2k_\lambda x))\nabla \hat{c}), \quad (6)$$

where $E_{ac} = \frac{p_a^2}{4\rho_0 c_0^2}$ is the acoustic energy density inside the channel. $\hat{\rho}$ and \hat{c} are defined as $\frac{\rho_0}{\rho_{avg}}$ and $\frac{c_0}{c_{avg}}$. ρ_{avg} and c_{avg} are the average density and average velocity of sound of the fluid domain calculated from mean temperature $(T_H + T_L)/2$. The gradient in density $\nabla \hat{\rho}$ and speed of sound $\nabla \hat{c}$ in this heat transfer study is only due to temperature gradient, so Eq. (6) can be written in terms of temperature gradient and it takes the form

$$f_{ac} = -E_{ac} \nabla T \left(\cos(2k_\lambda x) \frac{1}{\rho_{avg}} \frac{\partial \rho_0}{\partial T} + (1+\cos(2k_\lambda x)) \frac{1}{c_{avg}} \frac{\partial c_0}{\partial T} \right). \quad (7)$$

The above equation is used as a body force term in Navier-Stokes Eq. (2). The magnitude of streaming velocity can be written as $v_{str} \approx \frac{3v_a^2}{8c_0}$, where v_a is the amplitude of the first-order velocity \mathbf{v}_1 and c_0 is the speed of the sound [26]. For a channel filled with water at $E_{ac} = \frac{\rho_0 v_a^2}{2} = E_{ac} = 50 \text{ J/m}^3$, $\rho_0 \approx 1000 \text{ kg/m}^3$, and $c_0 \approx 1500 \text{ m/s}$, we get $v_a \approx 0.316 \text{ m/s}$. The resulting streaming velocity is in the order of $\approx 25 \mu\text{m/s}$, which is two orders of magnitude less compared to the velocity

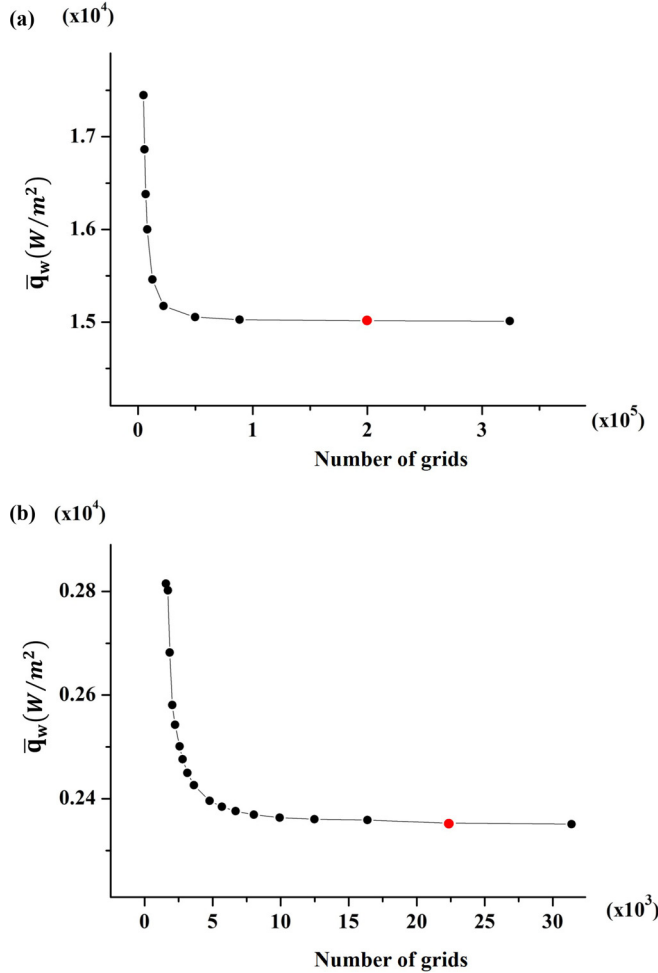


FIG. 4. Grid independence test for heat flux in ethanol. (a) Acoustic wave perpendicular to the direction of heat transfer. (b) Acoustic wave parallel to the direction of heat transfer. The red dot indicates the number of grids chosen, resulting in a fine computational mesh for above dependent variables to reach convergence.

due to acoustic body force ≈ 1 cm/s obtained in simulations. Hence the boundary-driven acoustic streaming phenomenon is neglected in this paper.

D. Numerical implementation

The system of governing equations Eqs. (1)–(3) is solved numerically using a finite difference scheme, and acoustic force density Eq. (7) is substituted as a body force term in the Navier Stokes equation. All the time-dependent heat transfer studies presented in this paper are carried out in a finite element method-based solver COMSOL MULTIPHYSICS 5.4. The heat transfer in the minichannel using acoustic body force is studied and solved by coupling a predefined laminar flow module and heat transfer module. The evolution of velocity field, temperature field, and heat flux are captured by employing a backward differential formulation with an adaptive time-stepping scheme based on local error estimates. Mesh convergence analysis was performed as shown in Fig. 4 to determine the number of grids large enough for all dependent variables to converge, ensuring a mesh-independent result. Among the two fluids taken for the analysis, ethanol experiences

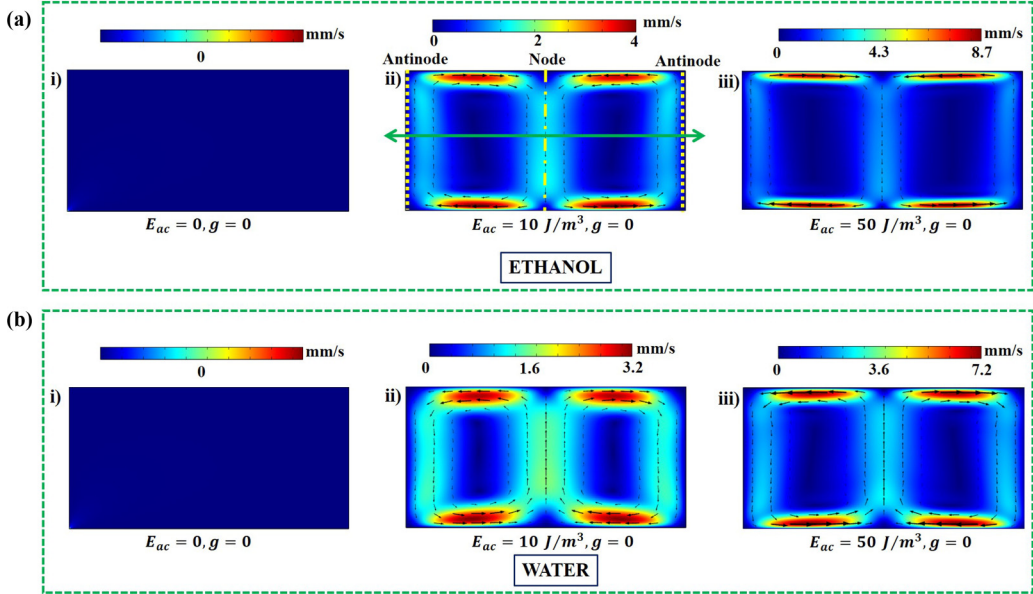


FIG. 5. Velocity profile due to acoustic forces at zero gravity condition. Standing acoustic wave is applied perpendicular to the direction of heat transfer. (a) Ethanol and (b) water. The green arrow indicates the direction of the standing acoustic wave.

maximum velocity for any given acoustic energy density. Hence, the grid independence test is done for ethanol at $E_{ac} = 50 \text{ J/m}^3$ with gravity. The number of triangular grids used for heat transfer enhancement is 198 910 (maximum element mesh size of about 0.02 mm) and suppression is 22 324 (maximum element mesh size of about 0.06 mm) beyond which the flow field and heat flux are unaffected by the increase in the number of grids. The consistent stabilization method is employed in COMSOL to reduce the Peclet number under unity by adding additional diffusive terms. Hence, the stability and accuracy of the problem are guaranteed by the robust stabilization methods (streamline diffusion and crosswind diffusion) in COMSOL.

IV. RESULTS AND DISCUSSION

In this section, we present the results demonstrating the proposed heat transfer mechanism in a minichannel using acoustic waves. The heat transfer enhancement is achieved when the applied acoustic wave is perpendicular to the direction of heat transfer. A modified Rayleigh number is proposed to take both acoustic and gravity force into account and the correlation is established for the heat transfer enhancement. Conversely, the acoustic force suppresses the heat transfer due to natural convection when the applied acoustic wave and direction of heat transfer are parallel to each other.

A. Standing wave applied perpendicular to the heat transfer direction: Heat transfer enhancement

Here, the ultrasonic standing wave is applied perpendicular to the direction of heat transfer as shown in Figs. 3(a) and 5(a-ii). Ethanol and water are employed as working fluids for the heat transfer analysis. The fluid flow and heat transfer behavior of both fluids are studied under two conditions. First, under the influence of only acoustic body force (without gravity) and then in the presence of both acoustic body force and buoyancy force due to gravity.

The velocity profile for ethanol and water in the presence of only acoustic body force for different acoustic energy densities can be seen in Figs. 5(a) and 5(b). The absence of acoustic force fails to create any fluid motion as shown in Figs. 5(a-i) and 5(b-i). In the cases of $E_{ac} > 0 \text{ J/m}^3$ and when the acoustic standing wave is applied perpendicular to the direction of heat transfer (heated bottom plate and cooled top plate) as shown in Figs. 5(a-ii), 5(a-iii), 5(b-ii), and 5(b-iii), the whole fluid domain is in an acoustically unstable configuration. Thus, acoustic force creates a steady fluid circulation in the entire domain which allows hot fluid from the bottom to reach the cold plate at the top to enhance the heat transfer. The magnitude of the acoustic body force is varied by varying the acoustic energy density E_{ac} and more energy density means more acoustic body force. Since the acoustic force is proportional to the temperature gradient and the temperature gradient [Eq. (7)] is more near the top and bottom walls, acoustic force produces a higher magnitude of velocities in those areas as shown in Figs. 5(a-ii), 5(a-iii), 5(b-ii), and 5(b-iii). It also must be noted that an increase in acoustic energy density results in higher fluid velocities. The velocity magnitude in ethanol is a bit higher compared to water, owing to the stronger acoustic force in ethanol compared to the water for the given energy density. Generally, acoustic streaming velocity is linearly proportional to acoustic body force, which is again linearly proportional to the energy density. Therefore, one would expect the acoustic streaming velocity to increase 5 times as we increase E_{ac} from 10 J/m^3 to 50 J/m^3 as shown in Fig. 5. However, from Fig. 5, it is clear that acoustic streaming velocity is not linearly proportional to acoustic force density. This nonlinear behavior can be easily explained once we take temperature profile coupling into consideration. Acoustic body force is linearly proportional to both E_{ac} and ∇T . Once E_{ac} is increased, acoustic body force tries to increase the velocity, the increase in velocity reduces the temperature gradient near the top and bottom walls due to more convection transport. The increase in E_{ac} is always accompanied by the reduction of ∇T ; this means acoustic body force will not be increased in a linear proportional manner. Hence, streaming velocity is not linearly proportional to the energy density in our problem.

The interesting observation in Fig. 5 is the direction of flow circulation for ethanol and water under the presence of acoustic forces. For ethanol, the fluid moves from the bottom to the nearest sidewall, sidewall to top, top to the center, and center to the bottom as shown in Figs. 5(a-ii) and 5(a-iii). This type of fluid flow circulation is referred to as BSTCB (bottom \rightarrow sidewall \rightarrow top \rightarrow center \rightarrow bottom) configuration and it continues to exist as long as the acoustic force is applied. Since the acoustic force is symmetric about the nodes, the BSTCB flow configuration observed in ethanol is also symmetric about the nodal line or Y-axis line passing through the center whereas for water, the fluid moves from bottom to center, center to top, top to the sidewall, and sidewall to the bottom as shown in Figs. 5(b-ii) and 5(b-iii). This type of fluid flow circulation is referred to as a BCTS (bottom \rightarrow center \rightarrow top \rightarrow sidewall \rightarrow bottom) configuration and this BCTS configuration is also symmetric about the nodal line. The main reason for the ethanol and water to exhibit different flow patterns is the speed of sound property variation with respect to the temperature. In ethanol, the speed of the sound decreases with increase in temperature [27], and in water [17] the speed of the sound increases with increase in temperature in the working temperature limits as shown in Fig. 6. The flow pattern in ethanol and water are explained in detail in the next paragraph.

The difference in the flow patterns of ethanol (BSTCB) and water (BCTS) can be explained by understanding the nature of acoustic force and its dependence on the speed of the sound and density of the fluid. The sign and relative magnitude of the terms $\frac{1}{\rho_{avg}} \frac{\partial \rho_0}{\partial T}$ and $\frac{1}{c_{avg}} \frac{\partial c_0}{\partial T}$ in the acoustic body force decide the type of fluid circulation. If the sign of both terms is the same (support each other) then the acoustic force moves the high density as well as the high speed of sound fluid portion to the center (node) or low density as well as low speed of sound fluid portion to sidewalls (antinode). If the sign of both terms is different (oppose each other), then the acoustic force moves either the higher density fluid or the higher speed of the sound fluid to the center based on whichever term dominates. More precisely, if the magnitude of the density term is higher than the speed of the sound term, then the higher density fluid will be pushed to the center (node) or lesser density fluid to the

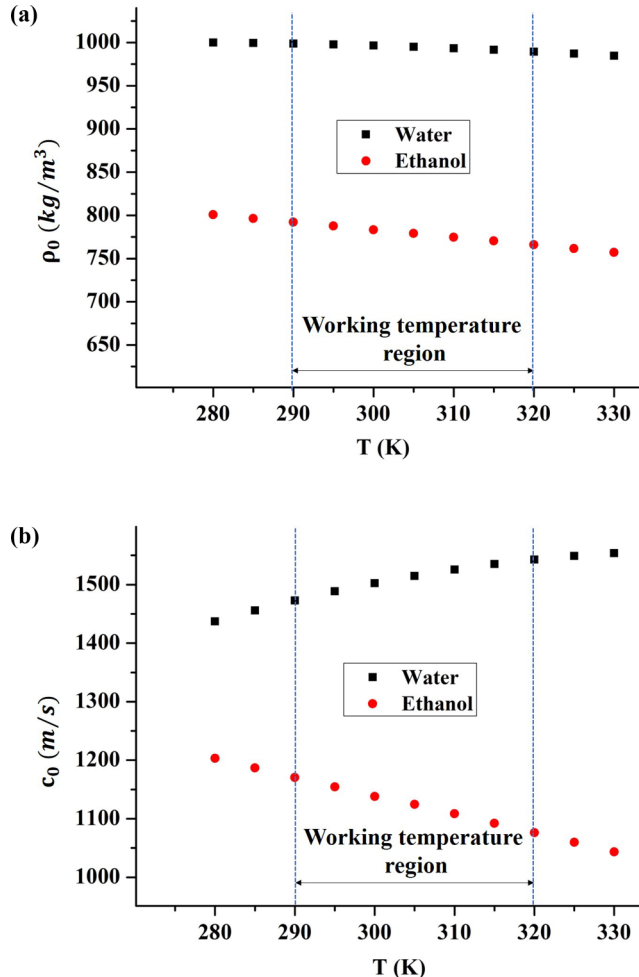


FIG. 6. Acoustic properties of ethanol and water at different temperatures. (a) Density of water and ethanol at different temperatures and (b) velocity of sound in water and ethanol at different temperatures.

sidewalls (antinode). Similarly, if the magnitude of the speed of the sound term is higher than the density term, then the higher speed of the sound fluid portion will be moved to the center (node) or the lower speed of the sound fluid portion will be moved to the walls (antinode). Here, the gradients in speed of sound and density with respect to temperature for both fluids are calculated using the curve fit equation obtained from the data points shown in Fig. 6.

The variation of density and speed of sound at different temperatures for ethanol and water is shown in Figs. 6(a) and 6(b). First, the flow pattern in ethanol is explained. For ethanol, it can be observed that as temperature increases, both the density and the speed of sound in ethanol decreases [27,28] as shown in Figs. 6(a) and 6(b). Hence the sign of both the density term ($\frac{\partial \rho_0}{\partial T}$) and the speed of sound term ($\frac{\partial c_0}{\partial T}$) in ethanol are negative and they support (same sign) each other. Consequently, the high-temperature ethanol at the bottom wall, which has a lower density and lower speed of the sound, moves to the sidewall (antinode), whereas the low-temperature ethanol at the top wall which has a higher density and higher speed of the sound moves to the center (node) of the channel as shown in Fig. 7(a). This creates the BSTCB circulation in ethanol when subjected to an acoustic standing wave as shown in Figs. 5(a-ii) and 5(a-iii).

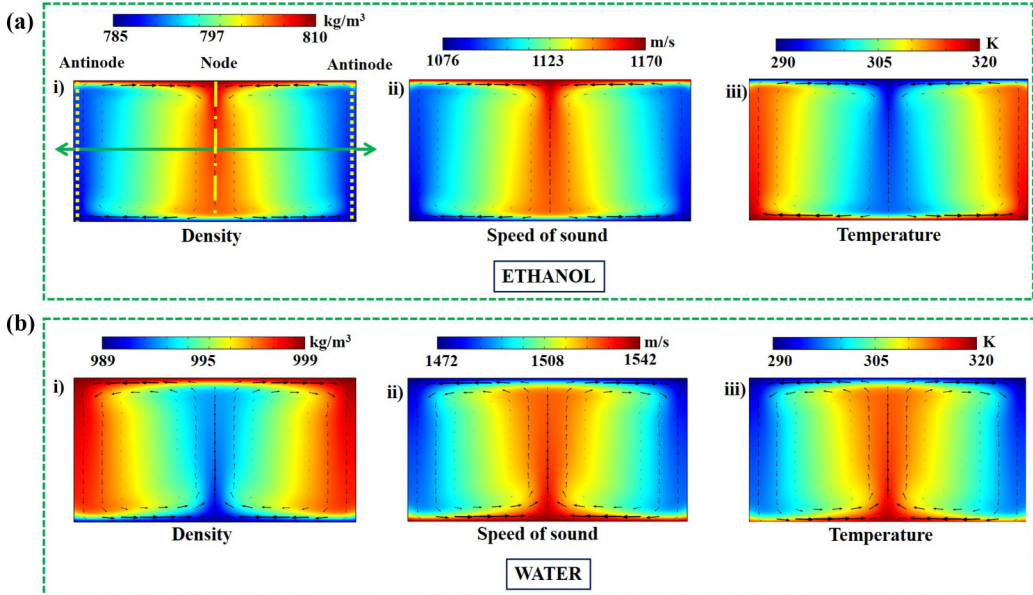


FIG. 7. Density, speed of sound, and temperature profile of ethanol and water at 50 J/m^3 when the acoustic wave is applied perpendicular to the direction of heat transfer. (a) Ethanol and (b) water.

Unlike ethanol, in water, the temperature rise corresponds to a rise in the speed of the sound [17] and a decrease in density [29] as shown in Figs. 6(a) and 6(b). Here the sign of the density term ($\frac{\partial \rho_0}{\partial T}$) is negative and the sign of the speed of sound, the term ($\frac{\partial c_0}{\partial T}$), is positive and so they oppose each other. For water, the magnitude of the term $\frac{1}{c_{\text{avg}}} \frac{\partial c_0}{\partial T}$ (0.0015 K^{-1}) dominates $\frac{1}{\rho_{\text{avg}}} \frac{\partial \rho_0}{\partial T}$ (-0.0003 K^{-1}). Due to the dominant speed of the sound term, the high-temperature water at the bottom wall which has a lower density and higher speed of the sound moves to the center (node) of the channel whereas the low-temperature water at the top wall which has higher density and lower speed of the sound moves to the sidewall (antinode), as shown in Fig. 7(b). This creates the BCTS_B circulation in water when subjected to an acoustic standing wave as shown in Figs. 5(b-ii) and 5(b-iii). This discussion provides a clear understanding for the different types of fluid circulation observed in ethanol (BSCB) and water (BCTS_B) under the influence of acoustic body force.

The velocity profile for ethanol and water in the presence of both acoustic body force and buoyancy force can be seen in Fig. 8. As we already discussed, when the acoustic standing wave is applied perpendicular to the direction of heat transfer, acoustic force moves hot fluid from the bottom to the top. Similar to acoustic force, the buoyance force also moves hot fluid from bottom to top due to gravity. Thus, the acoustic and buoyance forces support each other when the wave direction is perpendicular to the direction of heat transfer. Figures 8(a-i) and 8(b-i) show the velocity profile due to gravity (natural convection) without acoustic force ($E_{\text{ac}} = 0$, $g = 9.81 \text{ m/s}^2$) in ethanol and water, respectively. It must be noted that in the case of natural convection, the velocity field is unsteady [Figs. 8(a-i) and 8(b-i)]. Figures 8(a-ii), 8(a-iii), 8(b-ii), and 8(b-iii) show the flow pattern under the presence of both acoustic force and gravity ($E_{\text{ac}} > 0 \text{ J/m}^3$, $g = 9.81 \text{ m/s}^2$) in ethanol and water, respectively. In the presence of both acoustic force and gravity, steady flow behavior is emerged similar to the case of acoustic force without gravity, because at $E_{\text{ac}} = 10 \text{ J/m}^3$ and 50 J/m^3 the acoustic force dominates gravity.

The effect of energy density on spatiotemporal average heat flux for ethanol and water when the standing wave is applied perpendicular to heat transfer direction is shown in Figs. 9(a) and 9(b). The graph also compares the effects of acoustic body force without gravity and acoustic body force

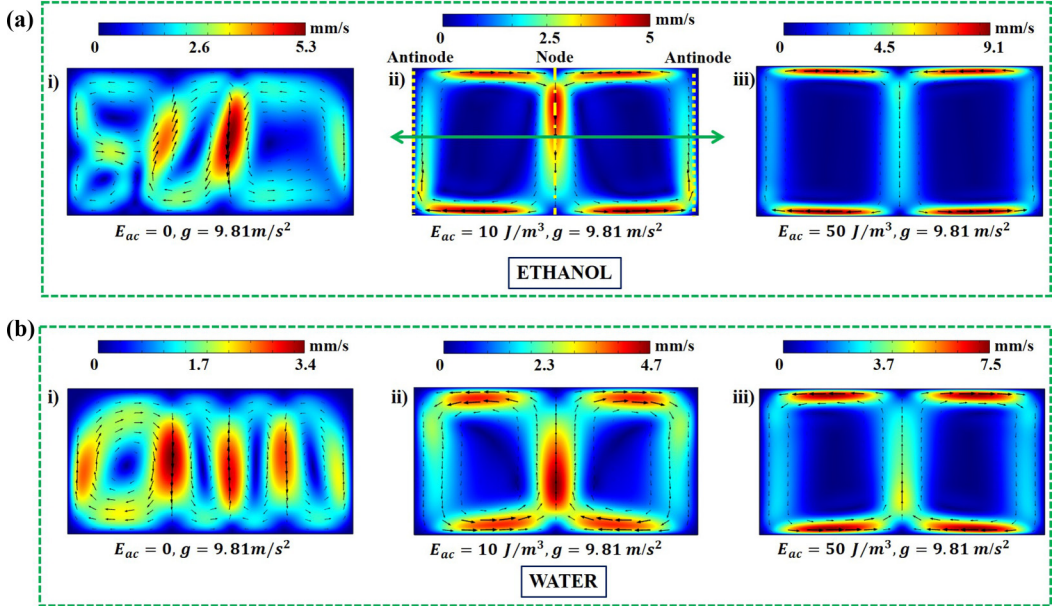


FIG. 8. Velocity profile due to the presence of both acoustics and gravity when the standing acoustic wave is applied perpendicular to the direction of heat transfer (a) ethanol and (b) water. The green arrow indicates the direction of the standing acoustic wave.

with gravity on heat transfer enhancement. In the case of acoustic force without gravity, the heat flux increases from conduction heat flux and keeps on increasing as we increase the acoustic energy density. If the acoustic force is applied along with gravity, then heat flux starts to increase from natural convection heat flux.

In the absence of both acoustic force and gravity, the conduction heat flux for ethanol is 1294.5 W/m^2 . When only acoustic force is applied, the net heat flux for ethanol rises up to 14521.5 W/m^2 , which is 11.2 times more than that of conduction heat transfer. When both acoustic force and gravity force are present, the net heat flux in ethanol rises up to 15024 W/m^2 as compared to natural convection heat flux 5998.91 W/m^2 . It must also be noted that, comparing to natural convection, though the velocity of the fluid is less at $E_{ac} = 10 \text{ J/m}^3$, the heat flux is more (Fig. 9). This is because, unlike buoyancy force, the acoustic body force induces fluid flow at a region of the channel where the temperature gradient is high (bottom wall) and so the heat transfer is effective. Acoustics along with gravity improves heat flux in ethanol up to 2.5 times compared to natural convection.

For water, the conduction heat flux for the given domain is 4620.47 W/m^2 . When only acoustic force is applied, the net heat flux rises up to 35726.23 W/m^2 , which is 7.7 times more than that of conduction heat transfer. When both acoustic force and gravity force are present, the net heat flux rises up to 36982.04 W/m^2 as compared to natural convection heat flux 16789.08 W/m^2 . Acoustics along with gravity improves heat flux up to 2.2 times compared to natural convection. From Figs. 9(a) and 9(b), it is clearly shown that when the acoustic force dominates the gravity the heat flux due to only acoustic force approaches the heat flux due to combined acoustic force and gravity at infinity [$(E_{ac} \rightarrow \infty) \Rightarrow (\bar{q}_w)_{ac} \rightarrow (\bar{q}_w)_{ac,g}$].

B. Characterization of heat transfer enhancement

If the force acting on the fluid domain is only gravity, then the conventional Rayleigh number Ra_g is sufficient to characterize the heat transfer due to natural convection. Here, apart from gravity,

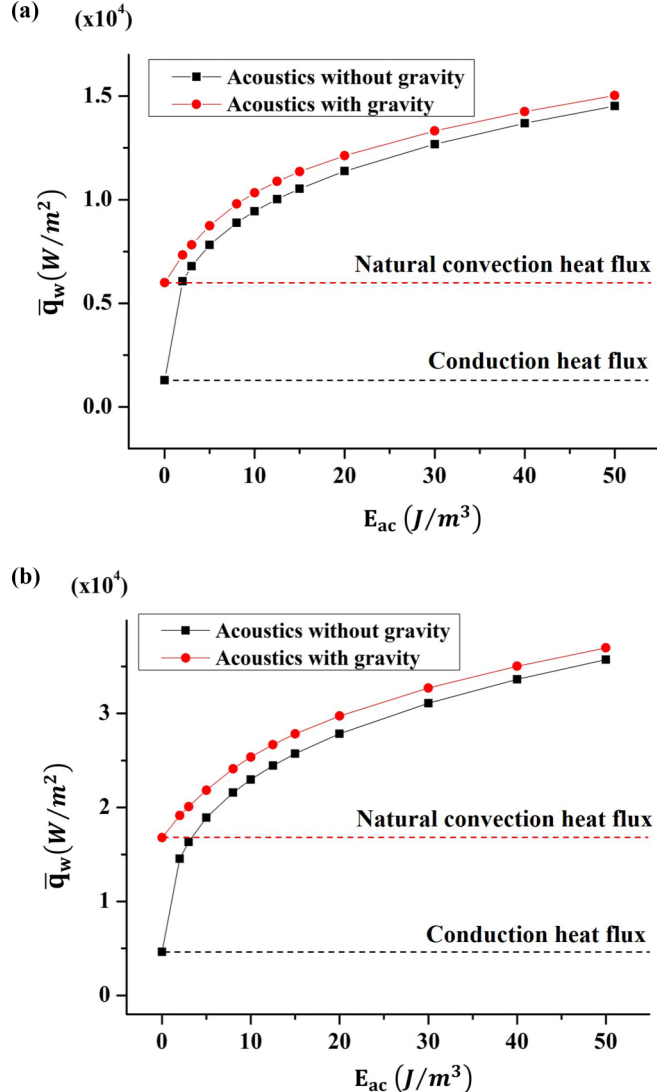


FIG. 9. Heat flux (spatiotemporal average) at different acoustic energy densities when the acoustic wave is applied perpendicular to the direction of heat transfer (a) ethanol and (b) water.

we have acoustic body force as well. So, we define a modified Rayleigh number Ra_m to take both the acoustic body force and buoyancy force into account. The Rayleigh number due to gravity Ra_g is given as [20]

$$\text{Ra}_g = \frac{\Delta\rho_0 gh^3}{\mu\alpha} = \frac{g\beta\Delta Th^3}{\nu\alpha}, \quad (8)$$

where $\Delta\rho_0 g$ is the body force due to gravity. Acoustic body force, which is symmetric about the nodal line, is given in Eq. (7) and can be scaled as $\frac{4E_{ac}}{w} \left(\frac{\Delta\rho_0}{\rho_0} + \frac{\Delta c_0}{c_0} \right)$. So, the Rayleigh number for acoustic body force Ra_{ac} can be written as

$$\text{Ra}_{ac} = \frac{2E_{ac}h^3}{\mu\alpha} \left(\frac{2\Delta\rho_0}{w\rho_0} + \frac{2\Delta c_0}{wc_0} \right) = -\frac{4E_{ac}h^3\Delta T}{w\mu\alpha}(\gamma + \beta). \quad (9)$$

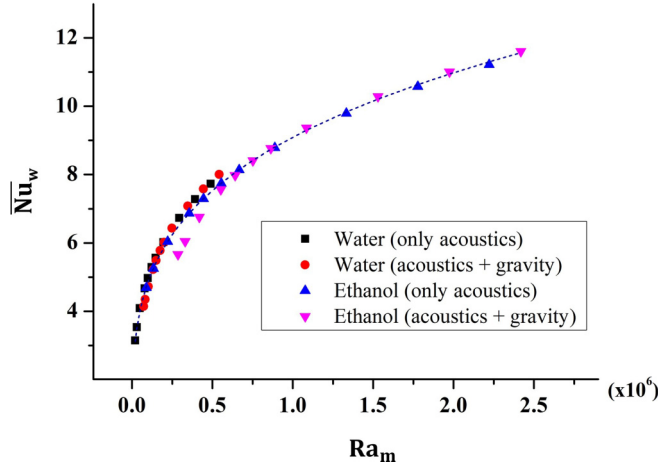


FIG. 10. Variation of Nusselt number (spatiotemporal average) for different modified Rayleigh numbers when the acoustic standing wave is perpendicular to the direction of heat transfer.

Here $\frac{\Delta\rho_0}{\rho_0} = -\beta\Delta T$, similarly $\frac{\Delta c_0}{c_0} = -\gamma\Delta T$, where β is thermal expansion coefficient and γ is the coefficient of the speed of sound.

The β and γ in the equation control the dynamics of heat transfer in the minichannel. Since the acoustic force and buoyancy force due to gravity support each other in the heat transfer

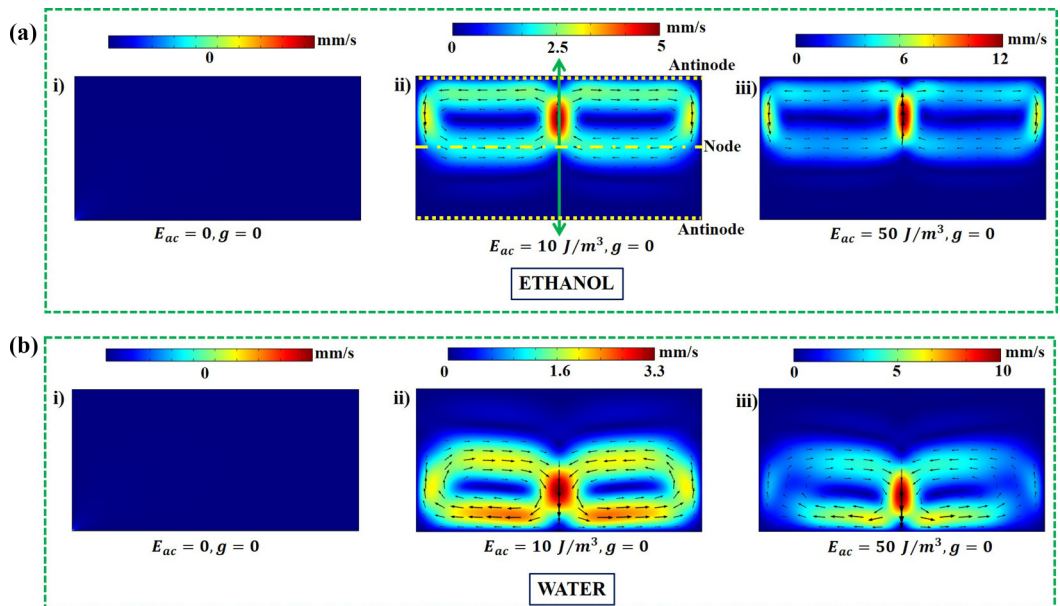


FIG. 11. Velocity profile due to acoustic forces at zero gravity condition. Standing acoustic wave is applied parallel to the direction of heat transfer. (a) Ethanol and (b) water. The green arrow indicates the direction of the standing acoustic wave.

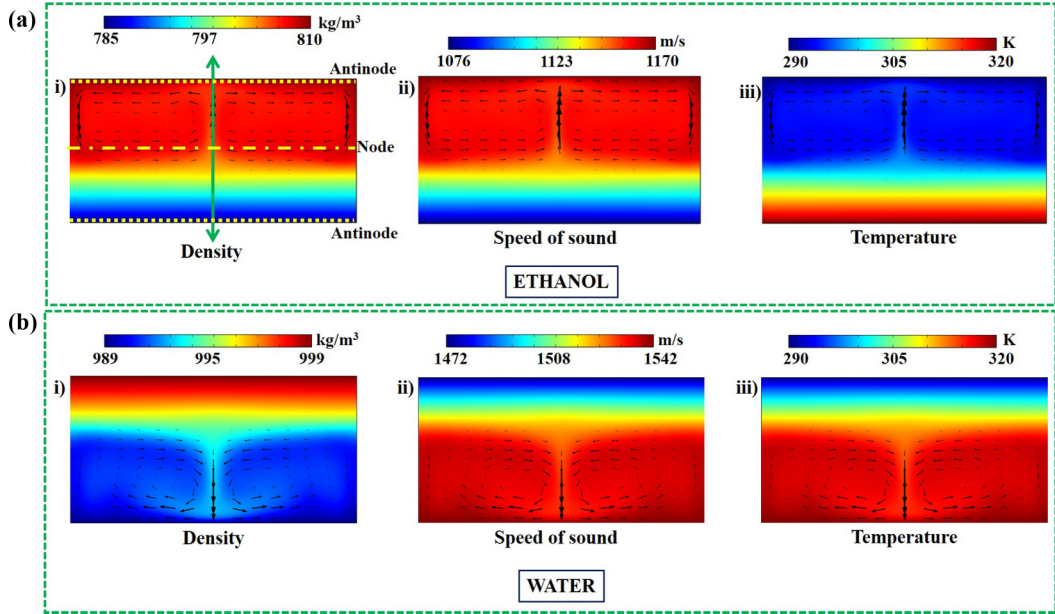


FIG. 12. Density, speed of sound, and temperature profile of ethanol and water at 50 J/m^3 when the acoustic wave is applied parallel to the direction of heat transfer. (a) Ethanol and (b) water.

enhancement, we define the modified Rayleigh number as $\text{Ra}_m = |\text{Ra}_{\text{ac}}| + |\text{Ra}_g|$, which is

$$\text{Ra}_m = \frac{\Delta Th^3}{\nu\alpha} \left(\left| -\frac{4E_{\text{ac}}(\gamma + \beta)}{\rho_0 w} \right| + |g\beta| \right), \quad (10)$$

The modified Rayleigh number Ra_m used in the simulation ranges from 1.9×10^4 to 2.5×10^6 . Figure 10 shows the variation of the Nusselt number (spatiotemporal average) with respect to the modified Rayleigh number and the resulting power-law correlation is

$$\overline{\text{Nu}}_w = 0.21\text{Ra}_m^{0.272}. \quad (11)$$

The above correlation can be helpful in predicting the Nusselt number from the given parameters due to standing acoustic waves, when applied perpendicular to the direction of heat transfer.

C. Standing wave applied parallel to the direction of heat transfer: Suppression of natural convection

This section demonstrates the effect of acoustic body force on the heat transfer when the acoustic standing wave is applied parallel to the direction of heat transfer. In this case, the nodes are formed at the center (parallel to X axis) and antinodes are formed at the top and bottom walls as shown in Figs. 3(b) and 11. The temperature boundary conditions are the same as discussed in Sec. III A. The velocity profiles for ethanol and water in the presence of only acoustic body force are shown in Figs. 11(a) and 11(b). In this case, it must be noted that the fluid motion is only present in certain parts of the domain and absent in the remaining part. So, the fluid convection is not complete and not effective as shown in Fig. 11 when compared to the standing wave applied perpendicular to the heat transfer direction (Fig. 5). This incomplete convection is due to the interplay between temperature field and acoustic force which creates an acoustically stable configuration in one region of the domain and acoustically unstable configuration in the remaining region. Another interesting result from Fig. 11 is, in ethanol, the fluid flow is absent at the bottom portion, and whereas in water, fluid

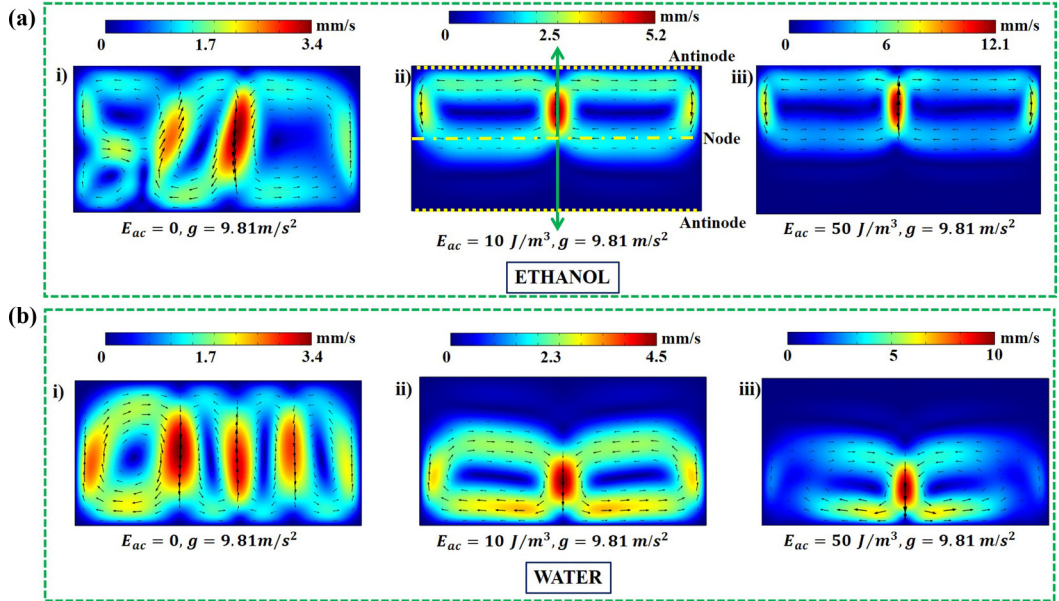


FIG. 13. Velocity profile due to the presence of both acoustics and gravity. Standing acoustic wave is applied parallel to the direction of heat transfer. (a) Ethanol and (b) water. The green arrow indicates the direction of the standing acoustic wave.

flow is absent at the top portion. The flow behavior of the ethanol and water shown in Figs. 11 and 12 is explained in detail in the next paragraph.

As discussed earlier (Fig. 6), for ethanol, the speed of sound term ($\frac{\partial c_0}{\partial T}$) and density term ($\frac{\partial \rho_0}{\partial T}$) has the same negative sign. Hence the lower temperature ethanol has a higher speed of sound and higher density. An acoustically unstable configuration is created at the top portion, because lower temperature ethanol which has higher density and higher speed of the sound is present at the top plate or antinode [Fig. 12(a)]. Thus, this acoustically unstable region relocates or moves the fluid from the top region to the center or nodal line as shown in Fig. 12(a) whereas a stable configuration is created at the bottom region since the higher temperature ethanol has low density, and the low speed of the sound ethanol is present at the antinode or bottom plate. So, this acoustically stable configuration in the bottom region inhibits the fluid flow from the bottom to the channel center [Fig. 12(a)]. Thus, in ethanol, fluid motion is present only in the top portion and absent in the bottom portion.

In the case of water, the speed of sound term ($\frac{\partial c_0}{\partial T}$) is positive and the density term ($\frac{\partial \rho_0}{\partial T}$) is negative. Thus, the lower temperature ethanol has a lower speed of sound and higher density. As the speed of sound term ($\frac{1}{c_{avg}} \frac{\partial c_0}{\partial T}$) has a higher magnitude than the density term ($\frac{1}{\rho_{avg}} \frac{\partial \rho_0}{\partial T}$), the dominating parameter is the speed of the sound. Hence, the higher speed of sound present at the node and lower speed of sound at the antinode is an acoustically stable configuration. At the bottom region, an unstable configuration is created due to the presence of high-temperature water, which has a higher speed of sound at the bottom plate or antinode [Fig. 12(b)]. An acoustically stable configuration is created at the top region due to the presence of low-temperature water which has a lower speed of sound at the top plate or antinode [Fig. 12(b)]. Thus, unlike ethanol, in water, fluid motion is present only in the bottom portion and absent in the top portion.

Due to this phenomenon of obtaining both stable and unstable configurations inside a channel, the heat transfer enhancement is not as effective as in the case where an acoustic wave is applied perpendicular to the direction of heat transfer. Acoustic forces (without gravity) rises heat flux up to

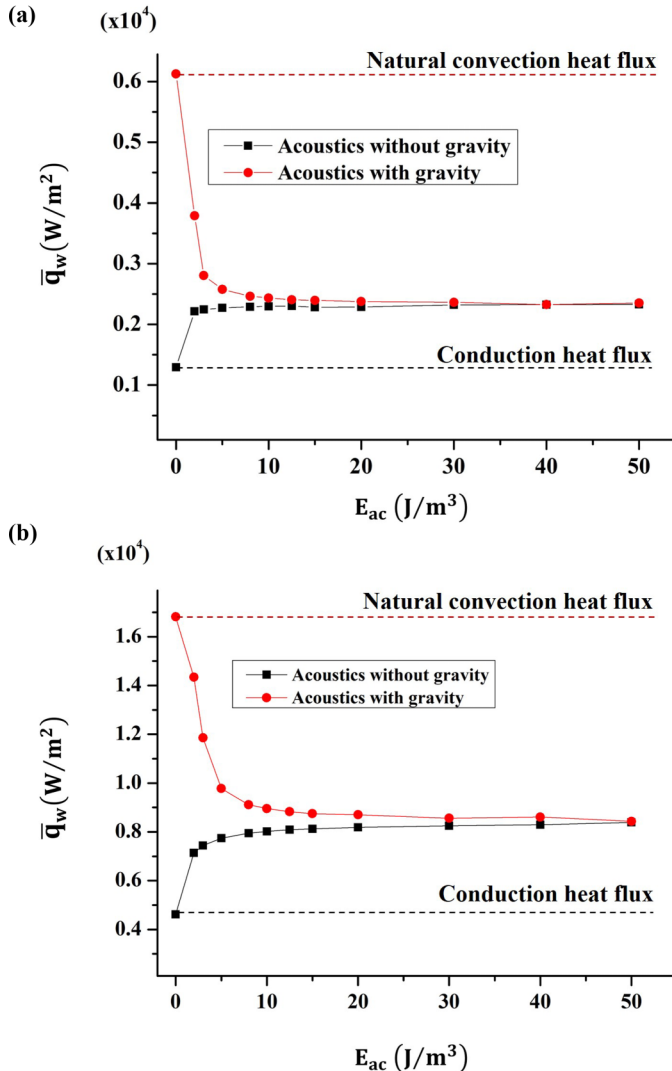


FIG. 14. Heat flux (spatiotemporal average) for different acoustic energy densities. Acoustic wave is applied parallel to the direction of heat transfer. (a) Ethanol and (b) water.

2328.8 W/m² in ethanol and 8392.42 W/m² in water. Thus, achieving an improvement of heat flux only by 1.8 times compared to the previous case (perpendicular).

In the presence of only gravity, buoyancy force sets fluid motion in the entire fluid domain as shown in Figs. 13(a-i) and 13(b-i), which results in natural convection heat flux 6124.5 W/m² and 16816.6 W/m² for ethanol and water, respectively, as shown in Figs. 14(a) and 14(b). When a standing acoustic half wave is applied parallel to the direction of heat transfer, the acoustic force opposes the buoyancy force in a certain part of the domain and supports in the other remaining part. Since the acoustic forces are stronger than buoyancy forces, the movement of the fluid in the corresponding half of the zone is arrested as shown in Figs. 13(a-ii), 13(a-iii), 13(b-ii), and 13(b-iii). In the presence of both acoustic force (parallel to the direction of heat transfer) and buoyancy force, the heat flux drops to 2362.12 W/m² for ethanol [Fig. 14(a)] and 8561.1 W/m² for water [Fig. 14(b)] at $E_{ac} = 30 \text{ J/m}^3$. Thus, the acoustic force when applied parallel to the heat

TABLE I. Summary of results showing effect of standing acoustic wave on heat transfer.

| Case No | Direction of applied acoustic force | Condition | Result |
|----------------|---|---------------------------|--|
| 1 | Perpendicular to the direction of heat transfer | Acoustics without gravity | Enhancement of heat transfer by 7.7 times in water and 11.2 times in ethanol compared to that of conduction heat transfer. |
| 2 | | Acoustics with gravity | Enhancement of heat transfer by 2.2 times for water and 2.5 times for ethanol compared to the natural convection. |
| 3 | Parallel to the direction of heat transfer | Acoustics without gravity | Enhancement of conduction heat flux by 1.8 times for both the fluids. |
| 4 | | Acoustics with gravity | Suppression of natural convection heat transfer by more than half for ethanol and by half for water. |

transfer direction shows much less improvement in heat transfer at zero gravity conditions and effective in suppressing the natural convection heat transfer due to gravity.

The effect of the standing acoustic half wave on heat transfer in a minichannel is summarized in Table I. The standing wave applied perpendicular to the heat transfer direction is very effective in heat transfer enhancement with or without the presence of gravity. Table I proves our hypothesis that

the acoustic relocation phenomenon can be employed as an effective heat transfer mechanism. Most importantly, this technique can serve as a potential cooling strategy of electronics in outer space under microgravity conditions where the natural convection heat transfer is not possible. In addition to these results, we have clearly explained the reason or logic behind it for a better understanding.

V. CONCLUSION

In this paper, a heat transfer mechanism based on the acoustic relocation phenomenon under the standing acoustic fields has been presented. The interplay among acoustic body force, velocity field, temperature field, and resulting heat transfer are clearly explained. The direction of the acoustic standing wave with respect to heat transfer direction is shown to play a major role in the heat transfer process. It is shown that heat transfer enhancement is effective when the acoustic wave is applied perpendicular to the heat transfer direction. Acoustic forces (without gravity) enhanced heat transfer remarkably up to 11 times compared to the heat transfer due to only conduction. Along with the gravity, acoustic force enhanced heat transfer up to 2.5 times compared to the natural convection. These results clearly show that the proposed heat transfer method using acoustic fields has great potential in the field of heat transfer. More specifically, in outer space under microgravity conditions where natural convection is absent, this proposed mechanism can be an excellent thermal management tool in cooling electronic devices. Interestingly, when the acoustic wave is applied parallel to the heat transfer direction, heat transfer enhancement is less effective in zero gravity conditions, whereas under the presence of gravity, the acoustic forces suppress the natural convection heat transfer by half.

- [1] S. M. Sohel Murshed and C. A. Nieto de Castro, A critical review of traditional and emerging techniques and fluids for electronics cooling, *Renew. Sustain. Energy Rev.* **78**, 821 (2017).
- [2] J. Meseguer, I. Pérez-Grande, and A. Sanz-Andrés, *Spacecraft Thermal Control* (Woodhead Publishing, Buckingham, England, UK, 2012).
- [3] A. Franco and C. Bartoli, Heat transfer enhancement due to acoustic fields: A methodological analysis, *Acoustics* **1**, 281 (2019).
- [4] S. Hyun, D.-R. Lee, and B.-G. Loh, Investigation of convective heat transfer augmentation using acoustic streaming generated by ultrasonic vibrations, *Int. J. Heat Mass Transf.* **48**, 703 (2005).
- [5] G. P. Chini, Z. Malecha, and T. D. Dreeben, Large-amplitude acoustic streaming, *J. Fluid Mech.* **744**, 329 (2014).
- [6] G. Michel and G. P. Chini, Strong wave–mean-flow coupling in baroclinic acoustic streaming, *J. Fluid Mech.* **858**, 536 (2019).
- [7] D. Zhou, D. Liu, X. Hu, and C. Ma, Effect of acoustic cavitation on boiling heat transfer, *Exp. Therm. Fluid Sci.* **26**, 931 (2002).
- [8] Y. Iida and K. Tsutsui, Effects of ultrasonic waves on natural convection, nucleate boiling, and film boiling heat transfer from a wire to a saturated liquid, *Exp. Therm. Fluid Sci.* **5**, 108 (1992).
- [9] S. Deshmukh, Z. Brzozka, T. Laurell, and P. Augustsson, Acoustic radiation forces at liquid interfaces impact the performance of acoustophoresis, *Lab Chip* **14**, 3394 (2014).
- [10] J. T. Karlsen, P. Augustsson, and H. Bruus, Acoustic Force Density Acting on Inhomogeneous Fluids in Acoustic Fields, *Phys. Rev. Lett.* **117**, 114504 (2016).
- [11] P. Augustsson, J. T. Karlsen, H.-W. Su, H. Bruus, and J. Voldman, Iso-acoustic focusing of cells for size-insensitive acousto-mechanical phenotyping, *Nat. Commun.* **7**, 11556 (2016).
- [12] S. Karthick, P. Pradeep, P. Kanchana, and A. Sen, Acoustic impedance-based size-independent isolation of circulating tumour cells from blood using acoustophoresis, *Lab Chip* **18**, 3802 (2018).
- [13] C. Pothuri, M. Azharudeen, and K. Subramani, Rapid mixing in microchannel using standing bulk acoustic waves, *Phys. Fluids* **31**, 122001 (2019).

- [14] D. Van Assche, E. Reithuber, W. Qiu, T. Laurell, B. Henriques-Normark, P. Mellroth, P. Ohlsson, and P. Augustsson, Gradient acoustic focusing of sub-micron particles for separation of bacteria from blood lysate, *Sci. Rep.* **10**, 3670 (2020).
- [15] H. Lee, in *Thermoelectrics: Design and Materials* (John Wiley & Sons, Chichester, England, UK, 2016), pp. 323–352.
- [16] J. T. Karlsen and H. Bruus, Acoustic Tweezing and Patterning of Concentration Fields in Microfluidics, *Phys. Rev. Applied* **7**, 034017 (2017).
- [17] M. Chávez, V. Sosa, and R. Tsumura, Speed of sound in saturated pure water, *J. Acoust. Soc. Am.* **77**, 420 (1985).
- [18] A. Korosi and B. M. Fabuss, Viscosity of liquid water from 25 to 150°. measurements in pressurized glass capillary viscometer, *Anal. Chem.* **40**, 157 (1968).
- [19] C. Ould-Lahoucine, H. Sakashita, and T. Kumada, A method for measuring thermal conductivity of liquids and powders with a thermistor probe, *Int. Commun. Heat Mass Transfer* **30**, 445 (2003).
- [20] A. Bejan, in *Convection Heat Transfer* (John Wiley & Sons, Chichester, England, UK, 2013), pp. i–xxxiii.
- [21] J. D. Anderson, *Computational Fluid Dynamics: An Introduction* (Springer, Berlin, 1992), pp. 15–51.
- [22] M. M. Ganzarolli and L. F. Milanez, Natural convection in rectangular enclosures heated from below and symmetrically cooled from the sides, *Int. J. Heat Mass Transf.* **38**, 1063 (1995).
- [23] E. Hemachandran, S. Karthick, T. Laurell, and A. Sen, Relocation of coflowing immiscible liquids under acoustic field in a microchannel, *Europhys. Lett.* **125**, 54002 (2019).
- [24] H. Bruus, Acoustofluidics 7: The acoustic radiation force on small particles, *Lab Chip* **12**, 1014 (2012).
- [25] J. T. Karlsen, W. Qiu, P. Augustsson, and H. Bruus, Acoustic Streaming and its Suppression in Inhomogeneous Fluids, *Phys. Rev. Lett.* **120**, 054501 (2018).
- [26] H. Bruus, Acoustofluidics 10: Scaling laws in acoustophoresis, *Lab Chip* **12**, 1578 (2012).
- [27] R. Wegge, M. Richter, and R. Span, Speed of sound measurements in ethanol and benzene over the temperature range from (253.2 to 353.2) K at pressures up to 30 MPa, *J. Chem. Eng. Data* **60**, 1345 (2015).
- [28] J. Ortega, Densities and refractive indices of pure alcohols as a function of temperature, *J. Chem. Eng. Data* **27**, 312 (1982).
- [29] G. S. Kell, Density, thermal expansivity, and compressibility of liquid water from 0° to 150°. Correlations and tables for atmospheric pressure and saturation reviewed and expressed on 1968 temperature scale, *J. Chem. Eng. Data* **20**, 97 (1975).